This article has been accepted for publication in a future issue of this journal, but has not been fully edited. Content may change prior to final publication. Citation information: DOI 10.1109/TNSRE.2018.2869426, IEEE Transactions on Neural Systems and Rehabilitation Engineering

Comparison of Convolutive Kernel Compensation and Non-negative Matrix Factorization of Surface Electromyograms

Martin Šavc, *Member, IEEE*, Vojko Glaser, Jernej Kranjec, *Member, IEEE*, Imre Cikajlo, Zlatko Matjačić and Aleš Holobar, *Member, IEEE*

***Abstract*— We compared Non-negative Matrix Factorization (NMF) and Convolution Kernel Compensation (CKC) techniques for high-density electromyogram (hdEMG) decomposition. The experimental data was recorded from nine healthy persons during controlled single degree of freedom (DOF) wrist flexion-extension, supination-pronation and ulnar-radial deviation movements. We assembled identified motor units and NMF components into three groups. Those active mostly during the first and the second movement direction per DOF were placed in G1 and G3 group, respectively. The remaining components were nonspecific for movement direction and were placed in G2 group. In ulnar and radial deviation, the relative energies of identified cumulative motor unit spike strains (CST) and NMF components were similarly distributed among the groups. In other two movement types, the energy of NMF components in G2 group was significantly larger than the energy of CSTs. We further performed coherence analysis between CSTs and sums of NMF components in each group. Both decompositions demonstrated a solid match, but only at frequencies < 3 Hz. At higher frequencies, the coherence hardly exceeded the value of 0.5. Potential reasons for these discrepancies include negative impact of motor unit action potential shapes and noise on NMF decomposition.**

***Index Terms*— high-density surface EMG, Non-negative Matrix Factorization, Convolution Kernel Compensation, wrist movements, motor unit identification**

I. Introduction

FOR more than a century, electromyograms (EMG) have been a vital source of information. By measuring the electrical activities of motor units (MUs) in skeletal muscles, they provide direct insight into neural codes governing the human movements [10]. Indeed, electrical activity of MUs repeats and amplifies (by a factor of up to 1000) the activity of motor neurons [20]. In this process, the information about the motor neuron firing times is preserved, whereas the shapes of action potentials (APs) in MUs and motor neurons differ significantly [20, 9, 10]. Moreover, detected MUAPs depend on many factors, including the muscle anatomy, relative distance of uptake electrode to the MUs, volume conductor properties and many others [9, 10].

Technical limitations prevent isolated recordings of individual MUs. Even the most selective needle electrodes record superimposed activity of several concurrently active MUs [20, 9, 10]. Surface EMG electrodes are much less selective and record the activity of several tens of concurrently active MUs. For this reason, surface EMG has traditionally been considered an interferential signal that is easy to misinterpret.

In order to circumvent this limitation, different techniques for decomposition of surface EMG into constituent MUs contributions have been proposed [16, 17, 21, 7, 35, 33, 4, 3, 37]. Among them, Holobar and Zazula [15] were the first to propose convolutive mixing model of high-density EMG (hdEMG) and its decomposition by Convolution Kernel Compensation (CKC) technique. Up to date, CKC has remained the most validated decomposition technique [16, 17, 18, 19, 20, 21, 7, 31, 45, 9, 10] and had significant impact on many other hdEMG decomposition techniques [4, 3, 38, 37].

Decomposition to the level of MUs allows for complete cancelation of MUAP shapes and, thus, complete reconstruction of motor neuron firing patterns (neural codes). However, it usually comes with relatively high computational and experimental costs. In order to increase the number of identified MUs and ease their discrimination, hdEMG recordings are acquired by arrays of several tens of surface electrodes [15, 16, 17, 18, 20, 9, 10]. Acquisition of such a large number of EMG channels may prove difficult in experimental setups, especially outside the controlled laboratory environment.

Due to these reasons, simpler decomposition techniques that do not aim at full compensation of MUAPs have been proposed. Out of them, Non-negative Matrix Factorization (NMF) has been frequently used, e.g. in [5, 6, 43, 39, 28, 30, 46] to mention only a few studies. For example, in [22] the authors applied NMF to individual pairs of opposing movements (degrees of freedom - DOFs) and validated the resulting decomposition against measured forces during isometric [22] and dynamic contractions [23, 24]. In [34] the authors showed that, compared to bipolar recordings, the multichannel EMG recordings add

This study was supported by the Slovenian Research Agency (project J2-7357 - Exact quantification of muscle control strategies and co-activation patterns in robot-assisted rehabilitation of hemiparetic patients and Programme funding P2-0041)

M. Šavc, V. Glaser, J. Kranjec and A. Holobar are with Faculty of Electrical Engineering and Computer Science, University of Maribor, Maribor, Slovenia (e-mails: martin.savc@um.si, vojko.glaser@um.si, jernej.kranjec@um.si, ales.holobar@um.si)

I. Cikajlo and Z. Matjačić are with University Rehabilitation Institute, Republic of Slovenia - Soča, Ljubljana, Slovenia (e-mails: imre.cikajlo@ir-rs.si, zlatko.matjacic@ir-rs.si)

This article has been accepted for publication in a future issue of this journal, but has not been fully edited. Content may change prior to final publication. Citation information: DOI 10.1109/TNSRE.2018.2869426, IEEE Transactions on Neural Systems and Rehabilitation Engineering

very little to the extracted NMF components. Experiments in [1] validated the effectiveness of NMF in identification of simple hand postures whereas the study in [44] showed that the components, estimated by NMF and selected by using variance accounted for (VAF) measure could be activated voluntarily with high accuracy. The authors in [14] showed that patients with impaired motor functions exhibited fewer muscle synergies identified by NMF than healthy controls. When validating the NMF some of these publications tested the decomposed components against external measurements of force or position. Others took the decomposition as an accurate representation of muscle activity and did not validate it at all.

Although CKC and NMF decompositions have been independently tested in many different experimental setups, they have never been mutually compared on the same set of EMG measurements. In this study, we applied them to the hdEMG recordings of wrist movements performed by healthy subjects. Contrary, to CKC, NMF does not aim to directly reconstruct the MU activity and to fully compensate the MUAPs in hdEMG. Thus, the rationale behind this study was to investigate and quantify similarities and discrepancies among the estimated NMF components and the activities of MUs, identified by CKC. With the ground truth about the MU activation unknown, this quantification was based on mutual comparison of NMF and CKC decompositions.

II. METHODS

A. CKC-based identification of MU firing pattern and corresponding MSE

The A/D-converted hdEMG can be modelled by [15, 16]:

$$\mathbf{y}(n) = \mathbf{H}\bar{\mathbf{t}}(\mathrm{n}) + \boldsymbol{\omega}(\mathrm{n}) \tag{1}$$

where $\boldsymbol{y}(n) = [y_1(n) \dots y_M(n)]^T$ is a vector of M EMG channels, $\boldsymbol{\omega}(n) = [\omega_1(n) \dots \omega_M(n)]^T$is zero-mean noise and $\bar{\mathbf{t}}(n) = \left[t_1(n), t_1(n-1) \dots t_1(n-L+1) \dots\ t_J(n) \dots\ t_J(n-L+1)\right]^T$ stands for vectorized block of L samples from all the MU firing patterns. The firing pattern of the j-th MU is defined as [15, 16]:

$$t_{\mathrm{j}}(\mathrm{n}) = \sum\nolimits_{\mathrm{k}} \delta\left(n - \tau_{\mathrm{j}}(k)\right), \qquad j = 1 \dots J. \tag{2}$$

where $\delta(.)$ is the unit-sample pulse and the k-th MUAP of the j-th MU appears at time $\tau_j(k)$.

The $M \times NL$ mixing matrix $\mathbf{H}$ in (1) comprises the L-sample long MUAPs:

$$\mathbf{H} = \left[\mathbf{H}_1, \mathbf{H}_2 \dots \mathbf{H}_J\right] \tag{3}$$

where

$$\mathbf{H}_{\mathrm{j}} = \begin{bmatrix} h_{1j}(0) & \dots & h_{1j}(L-1) \\ \vdots & \ddots & \vdots \\ h_{Mj}(0) & \dots & h_{Mj}(L-1) \end{bmatrix}, \ \mathrm{j} = 1, \dots, \mathrm{J}. \tag{4}$$

and $h_{ij}(n)$ stands for the n-th sample of the j-th MU's MUAP, detected by the i-th uptake electrode.

In order to increase the decomposition performance, the vector $\boldsymbol{y}(n)$ may be substituted by vectorized block of K samples from EMG measurements [15, 16]:

$$\mathbf{y}(n) = [y_1(n), y_1(n-1), \dots, y_1(n-K+1) \dots y_M(n-K+1)]^T \tag{5}$$

CKC estimates the j-th MU firing pattern as [15, 16]

$$\hat{t}_j(n) = \mathbf{c}_{\hat{t}_j\mathbf{y}}^{\mathrm{T}} \mathbf{C}_{\mathbf{y}}^{-1} \mathbf{y}(n) \tag{6}$$

where $\mathbf{C}_{\boldsymbol{y}} = E(\boldsymbol{y}(n)\boldsymbol{y}^T(n))$ is the correlation matrix of the EMG measurements, $\mathbf{c}_{t_j\boldsymbol{y}} = E\left(t_j(n)\boldsymbol{y}^T(n)\right)$ is the cross-correlation vector between the j-th MU firing pattern and measurements $\boldsymbol{y}(n)$**,** and $E(.)$ stands for mathematical expectation. The method has been tested in many different experimental setups [16, 17, 18, 19, 20, 21, 31, 45, 9, 10, 47, 41, 29], also in moderate dynamic contractions [8, 11, 12, 26, 40] and yielded up to 70 simultaneously active MUs. Furthermore, Pulse-to-Noise (PNR) metric has been proposed in [21] for assessment of accuracy of each individual MU identification. PNR has been shown to increase monotonically with both sensitivity and specificity of MU firing identification, whereat the value of PNR > 30 dB corresponds to MU identification accuracy > 95 % [21]. This is valuable feedback information on the accuracy of CKC-based decomposition and considerable advantage over the NMF-based decomposition.

B. Non-negative matrix factorization

Non-negative matrix factorization as described in [27] addresses the problem of decomposing a matrix $\mathbf{Z}$ into a product of matrices $\mathbf{W}$ and $\mathbf{F}$:

$$\mathbf{Z}^{(\mathrm{M}\times\mathrm{N})} = \mathbf{W}^{(\mathrm{M}\times\mathrm{J})}\mathbf{F}^{(\mathrm{J}\times\mathrm{N})} \tag{7}$$

with a chosen number of components (sources) J whereat $\mathbf{Z}$, $\mathbf{W}$ and $\mathbf{F}$ contain only non-negative values [27]. J is often required to be much smaller than either the number of measurements M (rows) or the number of samples N (columns of $\mathbf{Z}$) [27].

The basic multiplicative NMF method [27] optimizes the decomposition with respect to mean square error (MSE) between $\mathbf{Z}$ and $\mathbf{WF}$. The method is simple to implement, however, it is slow and multiple repetitions of numerical optimization are required to converge to good results [13]. Several methods have been proposed to improve the speed of its convergence [2, 25]. In our tests, the alternating least squares NMF method [2] yielded the fastest and the most consistent

This article has been accepted for publication in a future issue of this journal, but has not been fully edited. Content may change prior to final publication. Citation information: DOI 10.1109/TNSRE.2018.2869426, IEEE Transactions on Neural Systems and Rehabilitation Engineering

convergence (results not shown) and was, thus, selected for EMG decomposition.

Noteworthy, surface EMG signals are not non-negative and there is extensive literature on their pre-processing before applying the NMF decomposition [22, 13]. These techniques differ slightly, but are all based on a similar approach. First, envelopes of the acquired surface EMG signals are estimated by applying low-pass filter to rectified or squared values of the EMG signals. The envelopes are then decomposed using the selected NMF algorithm into preselected number of components, which reflect applied forces [22], activation patterns [13] or muscle synergies [37].

We selected the method and model proposed in [22]. In this experimental paradigm, the *m*-th surface EMG signal $y_m(n)$ is squared and filtered with a box filter of size 200 ms:

$$z_m(n) = \frac{1}{2\Delta n + 1} \sum_{n_i=n-\Delta n}^{n+\Delta n} y_m^2(n_i) \quad (8)$$

where Δn is half of the filter length (in samples). The envelope values $\mathbf{Z}(n) = [z_1(n), z_2(n) \dots z_M(n)]$ are then modelled by the non-negative data model (7), whereat **W** comprises all the mixing vectors and **F** all the NMF components reflecting the muscle excitation. In our study, the columns of **W** were normalized and had the second norm equal to 1.

Muscle excitation is non-negative and fits well into assumptions of NMF. This implies that at least two components **F** need to be estimated per each DOF, i.e., one for each movement direction. The upper bound of the number of components per selected DOF is harder to define, especially, when more than two muscles are involved into joint movement. Theoretically, the number of components $\mathbf{F}(n)$ equals the number of muscle excitation primitives or muscle synergies [20]. Although some researchers reported that selecting large number of components produces useful and noisy components that can be easily differentiated [13], we found that the NMF with large number of components *J* often splits useful components into several subcomponents. Therefore, we tested the NMF decomposition with *J=2, 3, 4, 6, 8, 10 and 12* components, whereat the identified components were classified into different source groups and summed together to compensate the impacts of potentially too large *J* (see text below).

C. Experimental signals

Nine healthy young subjects (age 35 ± 4 years, height 1.77 ± 0.05 m, weight 80 ± 10 kg) participated to the study. The subjects received a detailed explanation of the study and gave written informed consent prior to participation. The study was conducted in accordance with the Declaration of Helsinki and was approved by local ethics committee. All the subjects performed wrist flexions-extensions. Six subjects performed also pronations-supinations and four subjects performed ulnar-radial deviation. In all these measurements, two measurements of each movement per subject were performed. The subjects followed the trapezoidal (2 s ramp up + 5 s plateau + 2s ramp down + 5 s rest) force profiles. In each measurement, we recorded ten repetitions of the selected movement (e.g., ten wrist flexions and ten wrist extensions). The entire measurement lasted around 260 seconds.

The hdEMG signals were recorded by two arrays of 5×13 electrodes with diameter of 1 mm and inter-electrode distance of 8 mm (OT Bioelettronica, Italy). Electrodes were fixed with adhesive foam on the upper third of the dominant forearm, with electrode columns circumferencing the forearm in approximately perpendicular direction to the muscle fibers. In each subject, the electrodes covered about three quarters of the forearm circumference. Recorded EMG signals were amplified, sampled at 2048 Hz and 12 bits resolution (USB EMG 2 amplifier, OT Bioelettronica, Italy) and saved in longitudinal single-differential mode for offline analysis. This resulted in 4×26 grid of 102 hdEMG measurements.

Universal Haptic Device (UHD) robot [32] was used to oppose the wrist movement with a torque between 0 of 7 Nm and to measure exerted muscle forces (Fig. 1). Measured forces were sampled at 200 Hz and 12-bits resolution (PCI-6023E, National Instruments Inc., USA), displayed online as a graphical feedback to the subject and stored for offline analysis. Special trigger signal has been recorded by both USB EMG 2 and UHD and used offline to synchronize and resample the EMG and force signals to 2048 Hz.

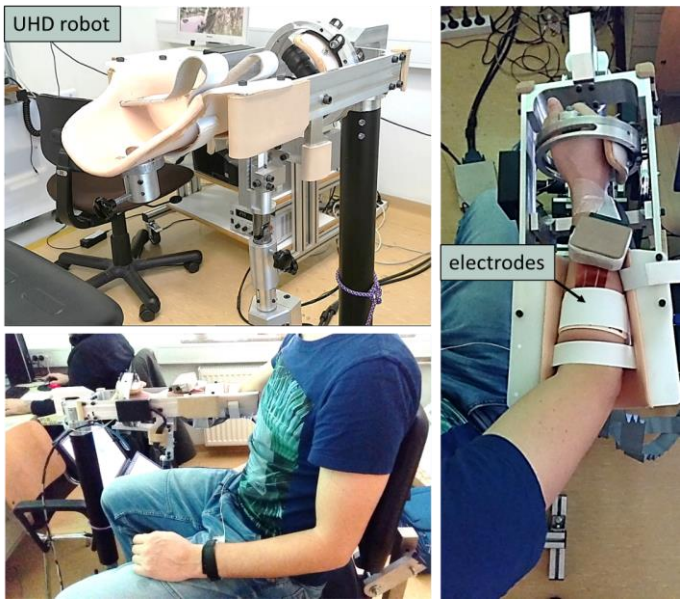

Fig. 1. UHD robot and experimental setup with two arrays of 12×5 electrodes mounted around the person's forearm.

D. Data analysis

All the EMG measurements were manually inspected before the NMF-based decomposition and the 0.82 ± 1.69 low quality EMG channels were discarded, on average. CKC method comes with automatic EMG channel selection. Therefore, no manual selection of EMG channels was performed for CKC-based decomposition. To further improve the signal quality, we performed manual analysis of movement artefacts, electrode-skin contact problems and mismatches between the reference

This article has been accepted for publication in a future issue of this journal, but has not been fully edited. Content may change prior to final publication. Citation information: DOI 10.1109/TNSRE.2018.2869426, IEEE Transactions on Neural Systems and Rehabilitation Engineering

and measured wrist forces. This analysis indicated higher signal quality in the last 120 s of the recorded signals. Therefore, we selected this epoch for the analysis. The NMF decomposed the whole segment, whereas CKC decomposed its 30 s long epochs, yielding both the MU firing patterns and corresponding MU filters that yielded these firings [16, 20]. Noteworthy, the 30 second long epochs were long enough to cover at least one movement in each direction (i.e. one flexion + one extension). We then applied the MU filter of each individual MU as identified on each 30 s long epoch to the entire 120 s of the EMG segment in order to identify the complete MU firing pattern. We mutually compared the resulting MU firing patterns and removed multiple identifications of the same MU by selecting the MU firing pattern with the highest PNR. In this way, we optimized the CKC decomposition time and guaranteed the identification of MUs recruited at different time moments.

In the case of CKC decomposition, only MUs with PNR > 30 dB (accuracy of decomposition > 95 %) [21] were considered for further analysis, whereas all the other MUs were discarded. For each DOF studied, identified MUs were classified into three different groups (Fig. 4). G1 group consisted of MUs that demonstrated at least 90% of firings in time intervals of the first movement direction (e.g. during flexion in flexion-extension DOF). G3 group comprised MUs with at least 90% of firings during the second movement direction (e.g. during extension in the flexion-extension DOF), whereas the remaining MUs were classified into G2 group.

We followed similar procedure in the case of NMF and classified all the $\mathbf{F}(n)$ components that exhibited at least 90 % of their energy during the first movement direction into G1 group, all the components that demonstrated at least 90 % of their energy during the second movement direction into G3 group and all the remaining components into G2 group (Fig. 4).

In each individual group, we summed up the identified MUs spike trains into cumulative spike train (CST) as it was demonstrated in [36] and further confirmed in [9, 10, 11, 12] that CST reflects linearly the descending drive to the muscle and significantly outperforms the EMG rectification.

Similarly, we applied the identified NMF mixing vectors $\widehat{\mathbf{w}}_j$ to nonfiltered versions of hdEMG measurements (we set $\Delta n = 0$ in (8)) and summed up the non-filtered $\mathbf{F}(n)$ components form the same group into cumulative $\mathbf{F}(n)$ component (CF). Afterwards, we used non-overlapping 1 s long Hanning windows to compute coherences between the CSTs and CFs in the same source group. Maximal coherence values were then analyzed in different frequency bands. The hypothesis of normal distribution was checked by Lilliefors test and rejected in 18 % of cases tested. We, therefore used Wilcoxon signed-rank test with significance level set to $P < 0.05$ to assess the statistical differences in coherences. We followed the same procedure when comparing the values of all the other reported metrics.

MUAP shapes were estimated by spike triggered averaging of hdEMG channels, using the identified MU firings as triggers. MUAP trains were calculated by convolving the MUAP shapes with the identified MU spike trains. Afterwards, the MUAP trains were summed across all the MUs in each group. Finally, the sums of MUAP trains in each MU group were squared and averaged across all the EMG channels. Coherences were then also computed between the averaged squared sum of MUAP trains and the CFs.

For all the MUs in the same source group, mean squared (MS) values of MUAPs were summed up in each hdEMG channel, yielding the spatial representation (in the space of hdEMG channels) of all the MUs in the group:

$$\boldsymbol{MS}_{\mathrm{MUAPs}}(i) = \sum_j \sum_n h_{ij}^2(n) \tag{9}$$

where $h_{ij}(n)$ stands for the n-th MUAP sample of the j-th MU in the group as detected by the i-th uptake electrode.

We used the same procedure for summing up the NMF's **w** vectors:

$$\boldsymbol{MS}_{\mathrm{w}}(i) = \sum_j \sqrt{\alpha_j}\,\widehat{\mathbf{w}}_j\ (i) \tag{10}$$

where $\widehat{\mathbf{w}}_j(i)$ stands for the i-th element of the j-th mixing vector $\widehat{\mathbf{w}}_j$ (i.e., the j-th column of the estimated $\mathbf{W}$) in the group and α_j is the energy of the j-th NMF component. Afterwards, we reordered $\boldsymbol{MS}_{\mathrm{MUAPs}}(i)$ and $\boldsymbol{MS}_{\mathrm{w}}(i)$ to match the topology of hdEMG electrodes and calculated their centroids. Finally, variance of signal accounted for by CKC-based decomposition was estimated by calculating the energy ratio between the sum of all the reconstructed MUAP trains $\hat{y}_m(t)$ and the original surface hdEMG channel $y_m(t)$:

$$VAF(\mathbf{y}, \hat{\mathbf{y}}) = 1 - \frac{\sum_{m,n}\left(y_m(n) - \hat{y}_m(n)\right)^2}{\sum_{m,n}\left(y_m(n)\right)^2} \tag{11}$$

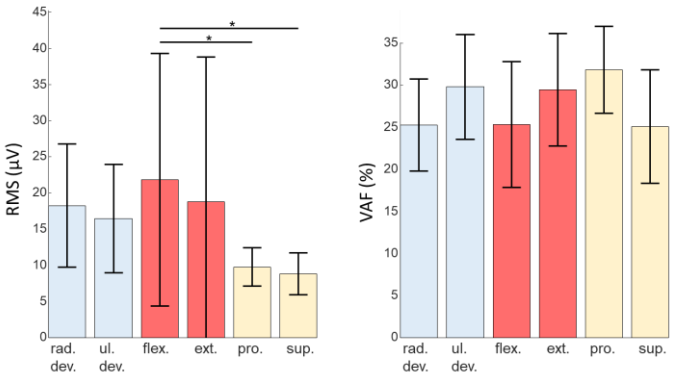

Fig. 2. Mean RMS values (μV) of recorded surface EMG signals during different movement types (*left*) and the Variance Accounted For (VAF) by CKC decomposition. We observed no significant differences between VAF values in different types of movement. The RMS values of recorded surface EMG was significantly higher in wrist flexion than in pronation and supination; flex. – flexion, ext. – extension, rad. dev. – radial deviation, ul. dev. – ulnar deviation, pro. – pronation, sup. – supination, * – Wilcoxon rank sum test ($p < 0.05$);

This article has been accepted for publication in a future issue of this journal, but has not been fully edited. Content may change prior to final publication. Citation information: DOI 10.1109/TNSRE.2018.2869426, IEEE Transactions on Neural Systems and Rehabilitation Engineering

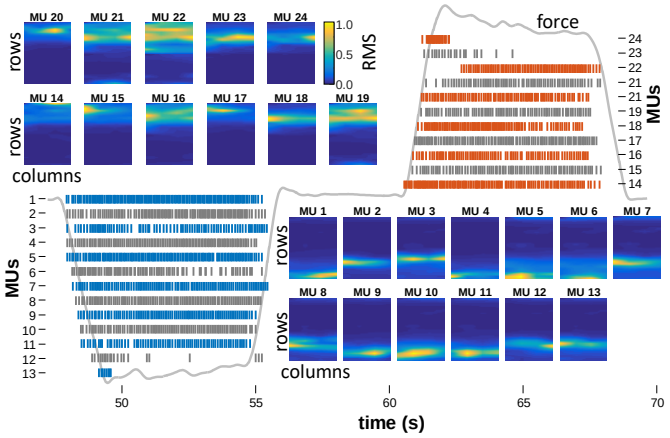

Fig. 3. Representative motor unit firing patterns identified by CKC decomposition during the wrist flexion and extension. Each vertical bar depicts one motor unit firing. For clarity reason, decomposition results of only one flexion and one extension repetition are shown. Normalized RMS maps of MUAPs depict the locations of identified MUs under the arrays of surface electrodes.

III. Results

Fig. 2 depicts the mean root-mean-square (RMS) values of recorded surface EMG signals during different movement types (*left*) and the Variance Accounted For (VAF) by CKC decomposition (*right*). Flexion yielded significantly higher RMS values than pronation and supination (Wilcoxon rank sum test, $p<0.05$), whereas no other RMS values were significantly different. We observed no significant differences between VAF values in different types of movement. Moreover, the average VAF values were comparable to the ones reported in the previous studies of CKC-based decomposition [15, 16, 17, 18, 19, 20, 21].

Fig. 3 depicts representative example of identified MU firing patterns during wrist flexion and extension. In total, 24 MSUs were identified with PNR ratio > 30 dB (accuracy > 95%). Thirteen of them were active during wrist extension (G3 group), the others were identified during flexion (G1 group). None of MUs were classified into G2 group. Fig. 3 also depicts RMS values of MUAPs (as assessed by spike-triggered averaging of the hdEMG signal and normalized to their maximum value per MU). The MUs identified during flexion and extension have clearly different spatial supports.

Fig. 4 depicts representative examples of CSTs and CF components for $J=12$, filtered with 200 ms long box filter. In contrast to CSTs, CFs from group G2 (and also from G1 and G3) demonstrate activity during both movement types. For clarity reasons, the squared sum of MUAP trains, averaged across the EMG channel is also depicted.

Fig. 5 depicts the total number of identified MUs and F components as a function of portion of energy during the first movement direction, whereas Fig. 6 depicts the relative energy of CSTs and CF components in G1-G3 groups for NMF with J=2, J=3, J=6 and J=12 components. For clarity reasons, we also depicted the average relative energy of CSTs and the corresponding MUAP trains. All the tested numbers of NMF components yielded relatively similar results. By using the Friedman test we did not identify any significant difference between their relative energies (Fig. 7) therefore, the NMF with $J=12$ components was analyzed in details as it provided the most flexibility in dividing the signal into the source groups.

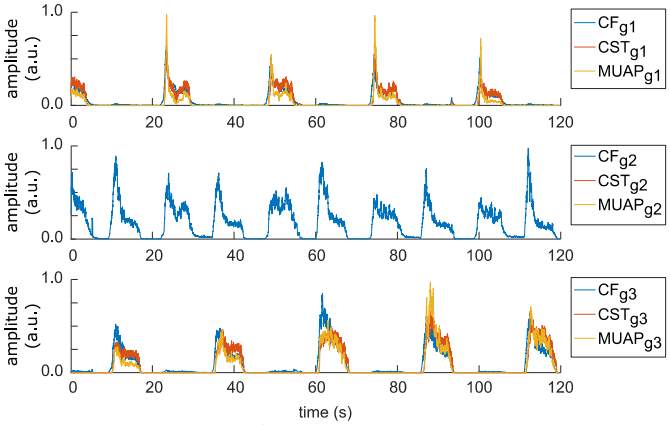

Fig. 4. Representative sums of NMF components (CFs), CSTs and squared sum of MUAP trains, averaged across all the EMG channels. NMF components, CSTs and MUAP trains were identified from hdEMG signals, acquired during extension-flexion task in individual subject.

In flexion-extension and radial-ulnar deviation, the CKC decomposition identified relatively low number of MUs in G2 group, whereas this was not the case for NMF (Fig. 5). The energy of identified MUs was distributed between G1 and G3 groups, whereas the energy of MUs in G2 group was relatively low, except in flexion-extension measurements 17 and 18 (Fig. 6). On the other hand, the CF components had the energy distributed among all the groups. In some measurements, the most of the energy was concentrated in G2 group (Fig. 6).

In pronation and supination, both decomposition methods identified the components in all three groups, though, when compared to the number of identified MUs, relatively large portion of NMF components and their energy was identified in G2 group (Figs. 5 and 6).

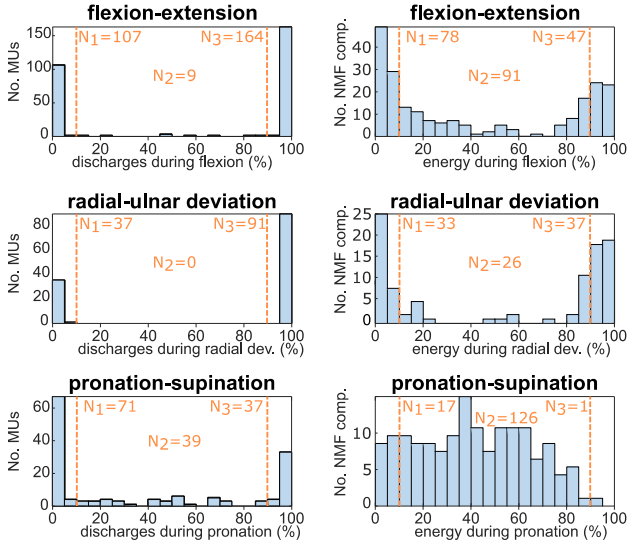

Fig. 5. Distribution of the number of identified MUs (left column) and NMF components (right column) with respect to different percentages of firings and energy in the first direction of each investigated DOF. The limits between the different groups of MUs/components are indicated by vertical dashed lines; N_i - the number of MUs or NMF components in the i-th group.

This article has been accepted for publication in a future issue of this journal, but has not been fully edited. Content may change prior to final publication. Citation information: DOI 10.1109/TNSRE.2018.2869426, IEEE Transactions on Neural Systems and Rehabilitation Engineering

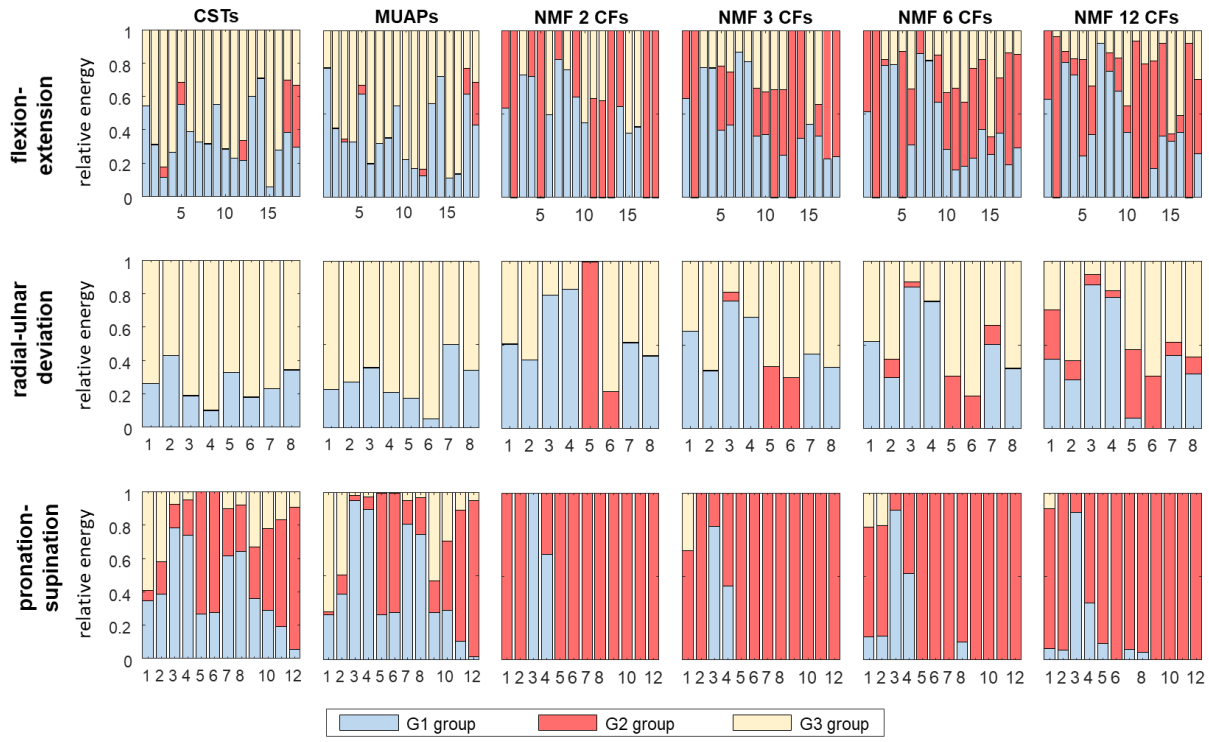

Fig. 6. Relative energy of identified CSTs, MUAP trains and CFs for NMF with J=2, 3, 6 and 12 components in G1, G2 and G3 groups per each performed hdEMG measurement.

Fig. 8 depicts the coherences (mean ± SD) in 5 Hz wide frequency bands between the NMF components and unfiltered CSTs (blue) and between the NMF components and the squared sum of identified MUAP trains, averaged across the EMG channels (red) in different groups (G1, G2 and G3) and different movement types. Coherence between the NMF components and unfiltered CSTs was frequently significantly lower than the coherences between the NMF components and the squared sum of identified MUAP trains (Wilcoxon signed-rank test, $p < 0.05$). This suggests that the identified NMF components did not fully compensate the MUAP shapes. Notwithstanding, G2 group yielded very low coherence values. These relatively low coherence values between CF and CST components indicated substantial discrepancies in the details of both decomposition results.

Fig. 9 depicts the maximum values of coherences between

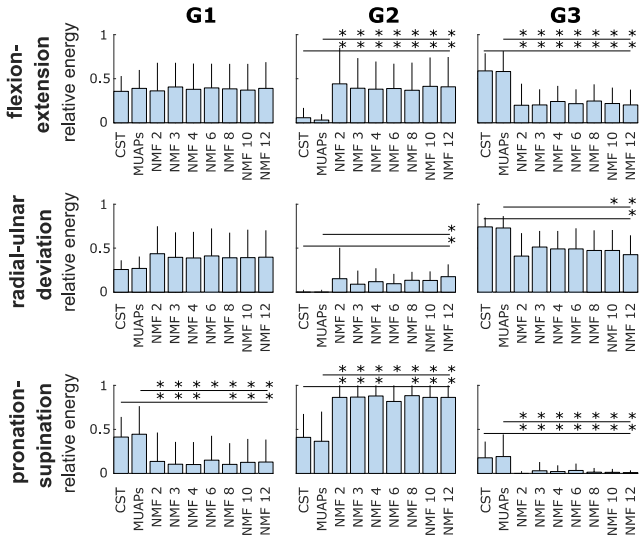

Fig. 7. Comparison of relative energies of CSTs, MUAP trains and CFs, identified by NMF algorithm with different number of components J=2, 3, 4, 6, 8, 10 and 12; * Friedman test, pairwise comparison with Bonferroni correction ($p < 0.05$).

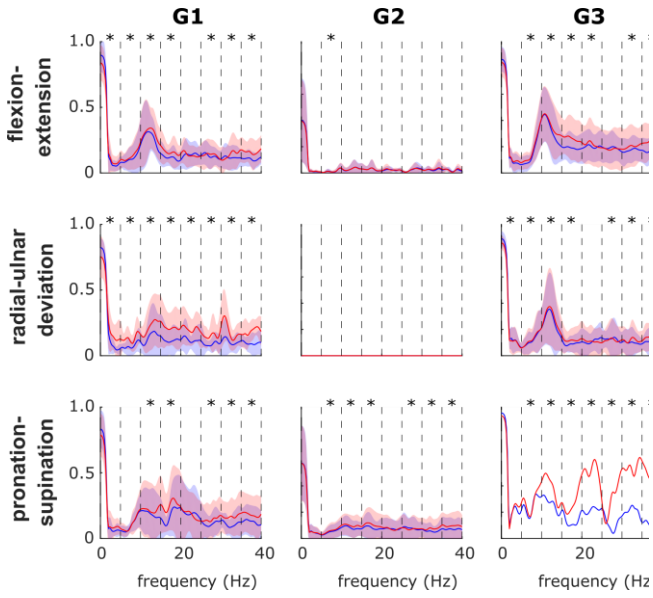

Fig. 8. Coherence (mean ± SD) between the NMF components and CSTs (blue) and between NMF components and the squared sum of identified MUAP trains, averaged across all the EMG channels (red) in different groups of sources (G1, G2 and G3) and in different movement types. Coherences in 5 Hz wide frequency bands were compared by Wilcoxon signed-rank test; * ($p < 0.05$);

This article has been accepted for publication in a future issue of this journal, but has not been fully edited. Content may change prior to final publication. Citation information: DOI 10.1109/TNSRE.2018.2869426, IEEE Transactions on Neural Systems and Rehabilitation Engineering

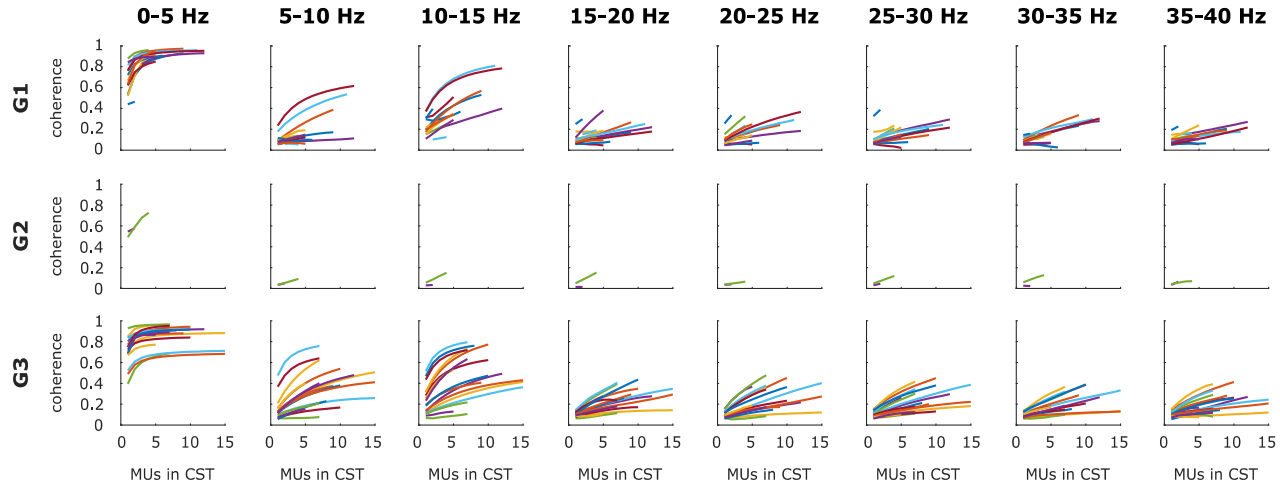

Fig. 9. Maximal coherence between CST and CF in different frequency bands as a function of MUs in CST during flexion-extension task. Different colored lines correspond to different hdEMG measurements.

the CFs and CSTs in different frequency bands as a function of the number of MUs in CSTs. For each depicted number of MUs in CST, all possible combinations of MUs in a group were used to generate the set of CSTs and the average coherence between this set and unfiltered CF was calculated. We then identified the maximum of these average coherences in each frequency band and reported it in Fig. 9. For most of the cases, the coherence values saturated relatively quickly with the number of MUs, indicating that the number of MUs identified in this study was sufficient to reliably estimate the coherences. In higher frequency bands, the values of coherence did not always saturate with the number of MUs. However, the depicted coherence trends suggest that the likelihood of coherence reaching values close to 1 when further increasing the number of identified MUs is relatively small. For clarity reasons, we provide only the results for flexion-extension movements. We obtained similar results for supination-pronation and ulnar-radial deviation movements (results not shown).

Fig. 10 depicts centroids of $\boldsymbol{MS_{MUAPs}}$ and $\boldsymbol{MS_{w}}$ maps in different wrist movements, accumulated across all the hdEMG measurements. Centroids of both decomposition methods were in good agreement, indicating that both techniques identified activity in the same spatial regions of surface hdEMG arrays. As expected, centroids of muscle excitation in the G1 group differed substantially from the centroids of muscle excitation in the G3 group. Centroids of muscle excitation in the G2 group (excitations that were non-specific for tested movement directions) were intermingled with centroids form the other two groups, indicating that different movement directions cannot be easily discriminated from raw hdEMG channels, even in the controlled experimental setups like ours.

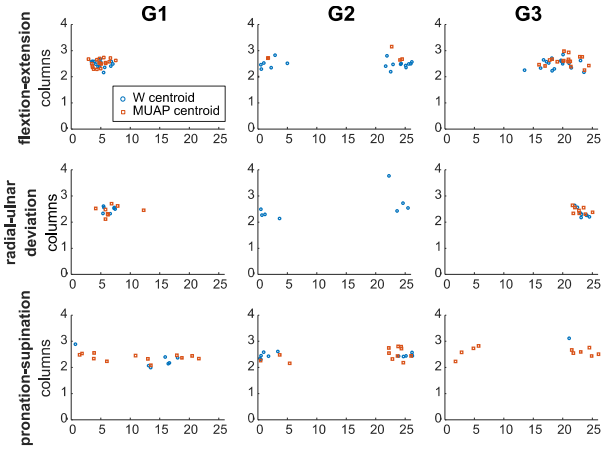

Fig. 10. Centroids of summed MS values of MUAPs and summed mixing vectors $\hat{\mathbf{w}}_j$ in each identified source group during different wrist movements. Presented results are accumulated across all the performed measurements. Electrode rows were approximately parallel to muscle fibers. Electrode columns were in circumferential direction.

IV. Discussion

We compared two popular methods for decomposition of hdEMG signals into muscle excitation primitives. A general overview of the methods is provided in Table I. Both methods can be used to assess activated muscle synergies [5, 6, 20] or exerted muscle forces [22, 23, 24, 20, 42], but differ substantially in the foreseen data model and its assumptions. NMF rectifies surface EMG signals and assumes that this rectification does not alter significantly the linearity of the mixing process in (1). On the other hand, CKC method exploits this mixing model and compensates MUAP shapes in order to directly estimate the MU firing patterns.

Both decomposition techniques identify subcomponents of a specific muscle excitation. CKC identifies individual MU firing patterns that need to be summed up to compensate the nonlinearities in the transfer functions of individual motor neurons [36, 11, 12]. For these reasons, we first classified the MUs into three complementary groups per investigated DOF (i.e. MUs active mostly during one movement direction, mostly during the opposite movement direction or during both movement directions) and, afterwards, calculated CST for each group. In NMF, we need to preselect the number of identified components. In this study, we tested different numbers of NMF components and empirically selected the decomposition with relatively large number of components (J = 12). This might result in identification of several subcomponents of specific

This article has been accepted for publication in a future issue of this journal, but has not been fully edited. Content may change prior to final publication. Citation information: DOI 10.1109/TNSRE.2018.2869426, IEEE Transactions on Neural Systems and Rehabilitation Engineering

TABLE I: COMPARISON OF NMF AND CKC PROPERTIES

Property	NMF	CKC
Required number of EMG channels per investigated muscle	≥ 1	≥ 20
Processing time per a second of EMG signals (measured on Intel i7 processor)	About 1 s	About 20 s
Complete compensation of MUAPs in isometric contractions	No	Yes
Complete compensation of MUAPs in dynamic contractions	No	No
Selectable number of components	Yes.	No, the number of identified motor units depends on the contraction level and quality of hdEMG signals.
Automatic assessment of decomposition accuracy	No	Yes
Decomposition into physiological components only	Not guaranteed	Guaranteed
Detection of superficial motor unit activity.	Moderate to good, depending on the number of EMG electrodes used	Good, as ≥ 20 electrodes are used per muscle
Detection of deep motor unit activity (within the detection volume of surface electrodes)	Moderate: many motor units contribute small MUAPs	Low: deep and small motor units are usually identified with questionable accuracy and, thus, removed by motor unit selection criteria (PNR > 30 dB in this study)
Automatic artefact detection and removal	No	Yes
Robustness to EMG outliers (recordings above the innervation zone, bad electrode-skin contact, extensive movement artefacts, etc.)	Moderate, depending on the number of EMG channels per muscle.	Good, as ≥ 20 electrodes are used per muscle and this guarantees sufficient redundancy of information and efficient outlier detection.

muscle excitation primitive. In order to compensate for this potential overestimation, we followed the same procedure as in the case of CKC decomposition and calculated cumulative NMF components in each of the aforementioned three source groups.

The results of both decompositions agreed well on a global scale, demonstrating that both techniques identify approximately the same global muscle activation patterns. On the other hand, the results differed substantially when we studied details of muscle excitation. The coherence between CFs and CSTs was mainly below 0.5 (Fig. 8). Moreover, NMF identified significantly larger portion of movement direction non-specific components (i.e. components in G2 group) than CKC (Fig. 5). In several cases, G2 group of NMF components accounted for the largest portion of the signal energy, also when clear separation of both movement directions was achieved by CKC (Fig. 6).

There are several possible reasons for these discrepancies. First, surface EMG and consequently CKC detects superficial MUs only. Deep MUs lay bellow the noise level and cannot be reliably identified by CKC (selection criterion of PNR > 30 dB in our study). This is, indeed, potential limitation of CKC that needs to be considered when interpreting the results of this study. According to our analysis, lowering the PNR threshold increased the number of identified motor units by one or two MUs, on average, whereas the identification accuracy of additional MUs and their impact on CST became highly questionable. Namely, while calculating CST, the MU contributions are weighted by the number of their firings. Inaccurately identified MUs may have a relatively big impact on CST. For these reason, we used relatively strict MU selection criteria. In addition, the average VAF for CKC-based decomposition (Fig. 2) was comparable to other hdEMG decomposition studies [16, 17, 18, 19, 20, 21, 7, 31, 45, 9, 10, 38, 4, 3, 37].

NMF does not put such a strict limit between identifiable and nonidentifiable components and likely yields activity of a larger number of MUs than CKC. However, the deep MUs have small MUAPs on the surface of the skin and likely contribute little to the identified NMF components. This conclusion is also supported by the results in Fig. 9. Most of the coherence values between CST and CF saturated or began to saturate before reaching the maximal number of identified MUs in CST, indicating that the conclusions of this study would likely not change considerably when more MUs were identified by CKC.

Second, CKC automatically removes the artefacts from the hdEMG signals, such as line inferences and movement artefacts; whereas (semi-) manual signal cleaning is required in the case of NMF as there is no guarantee that all the interferences will be automatically separated from the muscle excitation primitives. This may partially explain the low coherence values between CSTs and CFs in G2 group as this group likely gathered noisier NMF components that G1 and G3 groups. We have made considerable effort to ensure the good quality of hdEMG signals and reduce the impacts of noise. Thus, to our belief, the mismatch between CSTs and CFs in G2 group cannot be explained solely by noise.

Third, none of the tested decomposition techniques fully compensates for the MUAP changes due to dynamic muscle contractions, though in the case of investigated wrist movements these changes are relatively small, as previously discussed in [8]. Incomplete decomposition due to the negative

impact of MUAPs and, possibly, signal artefacts may lead to incomplete muscle crosstalk separation by NMF. This is supported by the results in Fig. 8, where the coherences between the NMF components and MUAP trains were frequently significantly higher than the coherences between the NMF components and CSTs. Note that both CSTs and MUAP trains were both identified by CKC and differ only in the exclusion/inclusion of MUAPs.

Fourth, we occasionally observed the narrow spike-like activity in the envelopes of the hdEMG signals. This activity appeared strictly at the beginning of each movement and was likely due to the movement artefacts and/or due to increased MU activity at the sudden initiation of the movement. Without the ground truth about the MU activity, we were not able to ascertain the origin of this activity. However, CKC method often reduced these spikes whereas NMF method projected them into the space of F components.

Noteworthy, NMF is faster than CKC and can be applied to a few surface EMG channels only, whereas CKC requires at least several tens of hdEMG channels per investigated muscle. Reference [34] showed that the results of NMF do not change significantly when hdEMG is used in place of a few EMG channels per muscle. Nevertheless, NMF does not track individual MUs and does not allow for detailed investigations of MU recruitment and derecruitment patterns and their adaptations in longer or/and repeated contractions (Figs. 3 and 4). The same applies to CSTs, computed from the individual MU spike trains. Thus, full decomposition to the level of MUs is required to fully analyze the excitation of skeletal muscles and its alternations due to fatigue, pathology or rehabilitation [20, 9, 10].

Finally, muscle co-activation patterns are difficult to assess from force recordings alone. Thus, we cannot easily classify the frequently observed NMF components from G2 group as methodological artefacts. In our case, MUs that were active during both wrist flexion and extension were identified by CKC in 5 out of 18 measurements. This demonstrates the intra-subject and intra-measurement variability of muscle control strategies, even in relatively simple tasks with clearly separated directions of recorded wrist forces. Moreover, we conducted this study on the forearm muscles and single degree-of-freedom wrist movements only and we cannot easily generalize the results to the other muscles and movement types. Nevertheless, the results of this study clearly demonstrate the discrepancies between both decomposition techniques and stress the need for their further systematic evaluation. The latter is a non-trivial task, especially in dynamic muscle contractions, where the ground truth about the muscle excitation is very difficult to assess.

In conclusion, we mutually compared two popular surface EMG decomposition techniques in controlled single-DOF wrist movements and quantified the discrepancies in their results. We showed that results of both decompositions agree on a global scale but differ substantially in several details. NMF identified significantly larger portion of direction non-specific components than CKC. Further investigations are required to fully understand the reasons for these discrepancies and to quantify their consequences for in vivo movement analysis of humans.

REFERENCES

[1] A. Ajiboye and R. Weir, "Muscle synergies as a predictive framework for the EMG patterns of new hand postures", Journal of Neural Engineering, vol. 6, no. 3, p. 036004, 2009.

[2] M. Berry, M. Browne, A. Langville, V. Pauca and R. Plemmons, "Algorithms and applications for approximate nonnegative matrix factorization", Computational Statistics & Data Analysis, vol. 52, no. 1, pp. 155-173, 2007.

[3] M. Chen, A. Holobar, X. Zhang and P. Zhou, "Progressive FastICA Peel-Off and Convolution Kernel Compensation Demonstrate High Agreement for High Density Surface EMG Decomposition", Neural Plasticity, vol. 2016, pp. 1-5, 2016.

[4] M. Chen and P. Zhou, "A Novel Framework Based on FastICA for High Density Surface EMG Decomposition", IEEE Transactions on Neural Systems and Rehabilitation Engineering, vol. 24, no. 1, pp. 117-127, 2016.

[5] A. d'Avella, P. Saltiel and E. Bizzi, "Combinations of muscle synergies in the construction of a natural motor behavior", Nature Neuroscience, vol. 6, no. 3, pp. 300-308, 2003.

[6] A. d'Avella, M. Giese, Y. Ivanenko, T. Schack and T. Flash, "Editorial: Modularity in motor control: from muscle synergies to cognitive action representation", Frontiers in Computational Neuroscience, vol. 9, 2015.

[7] D. Farina, A. Holobar, R. Merletti and R. Enoka, "Decoding the neural drive to muscles from the surface electromyogram", Clinical Neurophysiology, vol. 121, no. 10, pp. 1616-1623, 2010.

[8] D. Farina, Ning Jiang, H. Rehbaum, A. Holobar, B. Graimann, H. Dietl and O. Aszmann, "The Extraction of Neural Information from the Surface EMG for the Control of Upper-Limb Prostheses: Emerging Avenues and Challenges", IEEE Transactions on Neural Systems and Rehabilitation Engineering, vol. 22, no. 4, pp. 797-809, 2014.

[9] D. Farina and A. Holobar, "Human-Machine Interfacing by Decoding the Surface Electromyogram", IEEE Signal Processing Magazine, vol. 32, no. 1, pp. 115-120, 2015.

[10] D. Farina and A. Holobar, "Characterization of Human MUs From Surface EMG Decomposition", Proceedings of the IEEE, vol. 104, no. 2, pp. 353-373, 2016.

[11] J. Gallego, J. Dideriksen, A. Holobar, J. Ibáñez, J. Pons, E. Louis, E. Rocon and D. Farina, "Influence of common synaptic input to motor neurons on the neural drive to muscle in essential tremor", Journal of Neurophysiology, vol. 113, no. 1, pp. 182-191, 2014.

[12] J. Gallego, J. Dideriksen, A. Holobar, J. Ibanez, V. Glaser, J. Romero, J. Benito-Leon, J. Pons, E. Rocon and D. Farina, "The Phase Difference Between Neural Drives to Antagonist Muscles in Essential Tremor Is Associated with the Relative Strength of Supraspinal and Afferent Input", Journal of Neuroscience, vol. 35, no. 23, pp. 8925-8937, 2015.

[13] M. Gazzoni, N. Celadon, D. Mastrapasqua, M. Paleari, V. Margaria and P. Ariano, "Quantifying Forearm Muscle Activity during Wrist and Finger Movements by Means of Multi-Channel Electromyography", PLoS ONE, vol. 9, no. 10, p. e109943, 2014.

[14] N. Hesam-Shariati, T. Trinh, A. Thompson-Butel, C. Shiner and P. McNulty, "A Longitudinal Electromyography Study of Complex Movements in Poststroke Therapy. 2: Changes in Coordinated Muscle Activation", Frontiers in Neurology, vol. 8, p. 277, 2017.

[15] A. Holobar and D. Zazula, "Correlation-based decomposition of surface electromyograms at low contraction forces", Medical & Biological Engineering & Computing, vol. 42, no. 4, pp. 487-495, 2004.

[16] A. Holobar and D. Zazula, "Multichannel Blind Source Separation Using Convolution Kernel Compensation", IEEE Transactions on Signal Processing, vol. 55, no. 9, pp. 4487-4496, 2007.

[17] A. Holobar, D. Farina, M. Gazzoni, R. Merletti and D. Zazula, "Estimating motor unit discharge patterns from high-density surface electromyogram", Clinical Neurophysiology, vol. 120, no. 3, pp. 551-562, 2009.

[18] A. Holobar, M. Minetto, A. Botter, F. Negro and D. Farina, "Experimental Analysis of Accuracy in the Identification of Motor Unit Spike Trains From High-Density Surface EMG", IEEE Transactions on Neural Systems and Rehabilitation Engineering, vol. 18, no. 3, pp. 221-229, 2010.

[19] A. Holobar, V. Glaser, J. Gallego, J. Dideriksen and D. Farina, "Non-invasive characterization of motor unit behaviour in pathological tremor", Journal of Neural Engineering, vol. 9, no. 5, p. 056011, 2012.

[20] A. Holobar and D. Farina, "Blind source identification from the multichannel surface electromyogram", Physiological Measurement, vol. 35, no. 7, pp. R143-R165, 2014.
[21] A. Holobar, M. Minetto and D. Farina, "Accurate identification of motor unit discharge patterns from high-density surface EMG and validation with a novel signal-based performance metric", Journal of Neural Engineering, vol. 11, no. 1, p. 016008, 2014.
[22] N. Jiang, K. Englehart and P. Parker, "Extracting Simultaneous and Proportional Neural Control Information for Multiple-DOF Prostheses From the Surface Electromyographic Signal", IEEE Transactions on Biomedical Engineering, vol. 56, no. 4, pp. 1070-1080, 2009.
[23] N. Jiang, H. Rehbaum, I. Vujaklija, B. Graimann and D. Farina, "Intuitive, Online, Simultaneous, and Proportional Myoelectric Control Over Two Degrees-of-Freedom in Upper Limb Amputees", IEEE Transactions on Neural Systems and Rehabilitation Engineering, vol. 22, no. 3, pp. 501-510, 2014.
[24] N. Jiang, I. Vujaklija, H. Rehbaum, B. Graimann and D. Farina, "Is Accurate Mapping of EMG Signals on Kinematics Needed for Precise Online Myoelectric Control?", IEEE Transactions on Neural Systems and Rehabilitation Engineering, vol. 22, no. 3, pp. 549-558, 2014.
[25] J. Kim, Y. He and H. Park, "Algorithms for nonnegative matrix and tensor factorizations: a unified view based on block coordinate descent framework", Journal of Global Optimization, vol. 58, no. 2, pp. 285-319, 2013.
[26] T. Kapelner, N. Jiang, A. Holobar, I. Vujaklija, A. Roche, D. Farina and O. Aszmann, "Motor Unit Characteristics after Targeted Muscle Reinnervation", PLOS ONE, vol. 11, no. 2, p. e0149772, 2016.
[27] D. Lee and H. Seung, "Algorithms for Non-negative Matrix Factorization", in Advances in neural information processing systems, 2001, pp. 556-562.
[28] T. Lencioni, J. Jonsdottir, D. Cattaneo, A. Crippa, E. Gervasoni, M. Rovaris, E. Bizzi and M. Ferrarin, "Are Modular Activations Altered in Lower Limb Muscles of Persons with Multiple Sclerosis during Walking? Evidence from Muscle Synergies and Biomechanical Analysis", Frontiers in Human Neuroscience, vol. 10, p. 620, 2016.
[29] X. Li, A. Holobar, M. Gazzoni, R. Merletti, W. Rymer and P. Zhou, "Examination of Poststroke Alteration in Motor Unit Firing Behavior Using High-Density Surface EMG Decomposition", IEEE Transactions on Biomedical Engineering, vol. 62, no. 5, pp. 1242-1252, 2015.
[30] F. Lunardini, C. Casellato, A. d'Avella, T. Sanger and A. Pedrocchi, "Robustness and Reliability of Synergy-Based Myocontrol of a Multiple Degree of Freedom Robotic Arm", IEEE Transactions on Neural Systems and Rehabilitation Engineering, vol. 24, no. 9, pp. 940-950, 2016.
[31] H. Marateb, K. McGill, A. Holobar, Z. Lateva, M. Mansourian and R. Merletti, "Accuracy assessment of CKC high-density surface EMG decomposition in biceps femoris muscle", Journal of Neural Engineering, vol. 8, no. 6, p. 066002, 2011.
[32] J. Oblak, I. Cikajlo and Z. Matjacic, "Universal Haptic Drive: A Robot for Arm and Wrist Rehabilitation", IEEE Transactions on Neural Systems and Rehabilitation Engineering, vol. 18, no. 3, pp. 293-302, 2010.
[33] R. Merletti, M. Aventaggiato, A. Botter, A. Holobar, H. Marateb and T. Vieira, "Advances in Surface EMG: Recent Progress in Detection and Processing Techniques", Critical Reviews in Biomedical Engineering, vol. 38, no. 4, pp. 305-345, 2010.
[34] S. Muceli, N. Jiang and D. Farina, "Extracting Signals Robust to Electrode Number and Shift for Online Simultaneous and Proportional Myoelectric Control by Factorization Algorithms", IEEE Transactions on Neural Systems and Rehabilitation Engineering, vol. 22, no. 3, pp. 623-633, 2014.
[35] S. Nawab, S. Chang and C. De Luca, "High-yield decomposition of surface EMG signals", Clinical Neurophysiology, vol. 121, no. 10, pp. 1602-1615, 2010.
[36] F. Negro and D. Farina, "Linear transmission of cortical oscillations to the neural drive to muscles is mediated by common projections to populations of motoneurons in humans", The Journal of Physiology, vol. 589, no. 3, pp. 629-637, 2011.
[37] F. Negro, S. Muceli, A. Castronovo, A. Holobar and D. Farina, "Multi-channel intramuscular and surface EMG decomposition by convolutive blind source separation", Journal of Neural Engineering, vol. 13, no. 2, p. 026027, 2016.
[38] Y. Ning, X. Zhu, S. Zhu and Y. Zhang, "Surface EMG decomposition based on K-means clustering and convolution kernel compensation", IEEE journal of biomedical and health informatics, vol. 19, no. 2, pp. 471-477, 2015.
[39] S. Overduin, A. d'Avella, J. Roh and E. Bizzi, "Modulation of Muscle Synergy Recruitment in Primate Grasping", Journal of Neuroscience, vol. 28, no. 4, pp. 880-892, 2008.
[40] P. Povalej Bržan, J. Gallego, J. Romero, V. Glaser, E. Rocon, J. Benito-León, F. Bermejo-Pareja, I. Posada and A. Holobar, "New Perspectives for Computer-Aided Discrimination of Parkinson's Disease and Essential Tremor", Complexity, vol. 2017, pp. 1-17, 2017.
[41] J. Radeke, J. van Dijk, A. Holobar and B. Lapatki, "Electrophysiological method to examine muscle fiber architecture in the upper lip in cleft-lip patients", Journal of Orofacial Orthopedics / Fortschritte der Kieferorthopädie, vol. 75, no. 1, pp. 51-61, 2014.
[42] M. Sartori, U. Yavuz and D. Farina, "In Vivo Neuromechanics: Decoding Causal Motor Neuron Behavior with Resulting Musculoskeletal Function", Scientific Reports, vol. 7, no. 1, 2017.
[43] M. Tresch, V. Cheung and A. d'Avella, "Matrix Factorization Algorithms for the Identification of Muscle Synergies: Evaluation on Simulated and Experimental Data Sets", Journal of Neurophysiology, vol. 95, no. 4, pp. 2199-2212, 2006.
[44] S. Togo and H. Imamizu, "Empirical Evaluation of Voluntarily Activatable Muscle Synergies", Frontiers in Computational Neuroscience, vol. 11, p. 82, 2017.
[45] K. Watanabe, A. Holobar, M. Kouzaki, M. Ogawa, H. Akima and T. Moritani, "Age-related changes in motor unit firing pattern of vastus lateralis muscle during low-moderate contraction", AGE, vol. 38, no. 3, 2016.
[46] N. Wenger, E. Moraud, J. Gandar, P. Musienko, M. Capogrosso, L. Baud, C. Le Goff, Q. Barraud, N. Pavlova, N. Dominici, I. Minev, L. Asboth, A. Hirsch, S. Duis, J. Kreider, A. Mortera, O. Haverbeck, S. Kraus, F. Schmitz, J. DiGiovanna, R. van den Brand, J. Bloch, P. Detemple, S. Lacour, E. Bézard, S. Micera and G. Courtine, "Spatiotemporal neuromodulation therapies engaging muscle synergies improve motor control after spinal cord injury", Nature Medicine, vol. 22, no. 2, pp. 138-145, 2016.
[47] U. Yavuz, F. Negro, O. Sebik, A. Holobar, C. Frömmel, K. Türker and D. Farina, "Estimating reflex responses in large populations of MUs by decomposition of the high-density surface electromyogram", The Journal of Physiology, vol. 593, no. 19, pp. 4305-4318, 2015.